A&A 576, L2 (2015)
DOI: 10.1051/0004-6361/201425542

Astronomy & Astrophysics

Letter to the Editor

ALMA detection of [C II] 158 μm emission from a strongly lensed $z = 2.013$ star-forming galaxy*

D. Schaerer[1,2], F. Boone[2], T. Jones[3], M. Dessauges-Zavadsky[1], P. Sklias[1], M. Zamojski[1], A. Cava[1], J. Richard[4], R. Ellis[5], T. D. Rawle[6], E. Egami[7], and F. Combes[8]

[1] Observatoire de Genève, Département d'Astronomie, Université de Genève, 51 Ch. des Maillettes, 1290 Versoix, Switzerland
e-mail: daniel.schaerer@unige.ch
[2] CNRS, IRAP, 14 Avenue E. Belin, 31400 Toulouse, France
[3] Department of Physics, University of California, Santa Barbara, CA 93106, USA
[4] CRAL, Observatoire de Lyon, Université de Lyon 1, 9 avenue Ch. André, 69561 Saint-Genis Laval, France
[5] Department of Astronomy, California Institute of Technology, MS 249-17, Pasadena, CA 91125, USA
[6] ESAC, ESA, PO Box 78, Villanueva de la Cañada, 28691 Madrid, Spain
[7] Steward Observatory, University of Arizona, 933 N. Cherry Ave, Tucson, AZ 85721, USA
[8] Observatoire de Paris, LERMA, 61 Av. de l'Observatoire, 75014 Paris, France

Received 18 December 2014 / Accepted 11 February 2015

ABSTRACT

Aims. Our objectives are to determine the properties of the interstellar medium (ISM) and of star formation in typical star-forming galaxies at high redshift.
Methods. Following up on our previous multi-wavelength observations with HST, *Spitzer*, *Herschel*, and the Plateau de Bure Interferometer (PdBI), we have studied a strongly lensed $z = 2.013$ galaxy, the arc behind the galaxy cluster MACS J0451+0006, with ALMA to measure the [C II] 158 μm emission line, one of the main coolants of the ISM.
Results. Emission of the [C II] line from the southern part of this galaxy is detected at 10σ. Taking strong gravitational lensing into account, which provides a magnification of $\mu = 49$, the intrinsic lensing-corrected [C II] luminosity is $L_{[CII]} = 1.2 \times 10^8\ L_\odot$. The observed ratio of [C II]-to-IR emission, $L_{[CII]}/L_{FIR} \approx (1.2{-}2.4) \times 10^{-3}$, is found to be similar to that in nearby galaxies. The same also holds for the observed ratio $L_{[CII]}/L_{CO} = 2.3 \times 10^3$, which is comparable to that of star-forming galaxies and active galaxy nuclei (AGN) at low redshift.
Conclusions. We utilize strong gravitational lensing to extend diagnostic studies of the cold ISM to an order of magnitude lower luminosity ($L_{IR} \sim (1.1{-}1.3) \times 10^{11}\ L_\odot$) and SFR than previous work at high redshift. While larger samples are needed, our results provide evidence that the cold ISM of typical high-redshift galaxies has physical characteristics similar to normal star-forming galaxies in the local Universe.

Key words. galaxies: high-redshift – galaxies: ISM – galaxies: starburst

1. Introduction

Observations of CO molecular emission and fine structure lines, such as [C II] 158 μm, provide interesting insight into the gas reservoir and interstellar medium (ISM) of galaxies (Carilli & Walter 2013). Although these observations are now yielding first measures of the molecular gas fraction at high redshifts (e.g. Tacconi et al. 2010; Saintonge et al. 2013) and hints at the ISM (photo-dissociation regions (PDRs), and H II regions) up to $z \sim 6$ (Riechers et al. 2013, 2014; De Breuck et al. 2014; Rawle et al. 2014), very little is known about the properties of the most abundant galaxies with relatively low IR luminosities and modest stellar masses. Gravitationally lensed sources offer a unique chance to sample this regime.

The *Herschel* Lensing Survey of massive galaxy clusters (Egami et al. 2010) and accompanying multi-wavelength observations were in particular designed to constrain the properties of typical-luminosity galaxies by probing beyond nominal sensitivity limits with the power of strong gravitational lensing. Detailed stellar, star formation, and dust properties of a sample of seven galaxies at $z \sim 1.5{-}3$ were determined by Sklias et al. (2014). Using CO observations, we also studied their molecular gas properties in Dessauges-Zavadsky et al. (2015). In cycle 0, we were able to observe one of these galaxies with ALMA, the gravitationally lensed, multiply-imaged arc MACS J0451+0006 at $z = 2.013$, to study its ISM/PDR properties, as part of an ongoing ALMA program to study line emission in high-redshift gravitationally-lensed galaxies (PI: Ellis). We present here results concerning the [C II] 158 μm emission, providing some of the first information on [C II] and CO in an IR-faint ($L_{IR} \sim (1.1{-}1.4) \times 10^{11}\ L_\odot$), low-mass ($M_\star \sim 2.5 \times 10^9\ M_\odot$ for a Chabrier initial mass function, hereafter IMF) star-forming galaxy at high redshift.

The observational data are described in Sect. 2. Our main results are presented and discussed in Sect. 3. Section 4 summarizes our main conclusions. We adopt a Λ-CDM cosmological model with $H_0 = 70$ km s^{-1} Mpc^{-1}, $\Omega_m = 0.3$ and $\Omega_\Lambda = 0.7$.

* Based on ALMA observations 2011.0.00130.S.

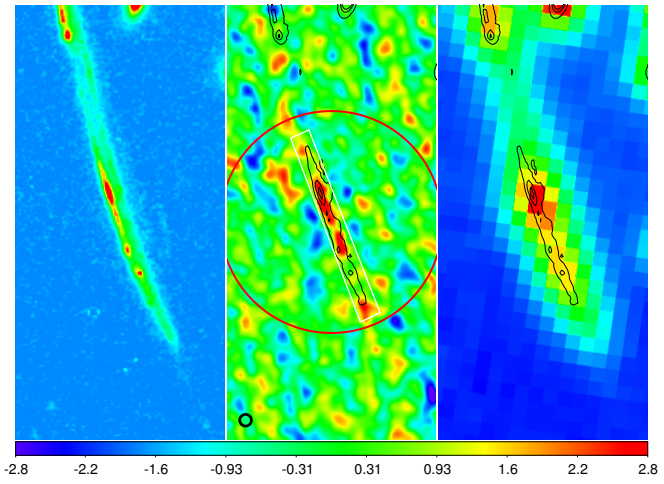

Fig. 1. *From left to right*: HST/WFC3 image in the filter *F140W*, ALMA [C II] 158 μm integrated map not corrected for primary beam attenuation, and *Spitzer* map with IRAC at 3.6 μm. Contours in the *middle and right panel* show the HST flux. The colour scale of the ALMA map is shown at the bottom in Jy km s^{-1}. To emphasize the emission from the arc, the ALMA data were tapered and the resolution is 0.5″ (represented by the black circle at the bottom left). The red circle represents the ALMA primary beam at half its maximum; its diameter is 9.5″. The white box delineates the region over which the continuum and the spectra have been integrated. The images are 9″ by 18″ side with a standard orientation (N up, E *left*).

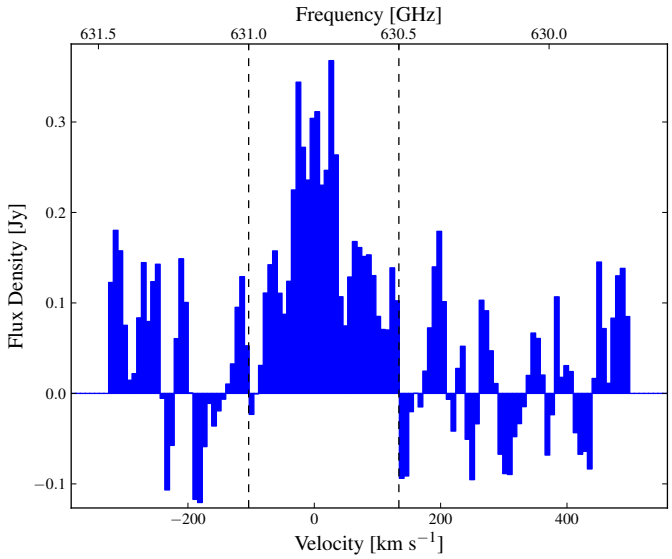

Fig. 2. Observed [C II] 158 μm spectrum obtained by integrating the data cube corrected for the primary beam in a box encompassing the southern part of the arc. The dashed vertical lines show the window within which the channels are summed to obtain the line flux. The Doppler velocities (lower axis) are computed with respect to the [C II] 158 μm frequency at $z = 2.013$, namely 630.78 GHz.

2. Observations

2.1. ALMA observations and results

The MACS J0451+0006 arc was targeted with ALMA in cycle 0 to map [C II] emission on ∼200 pc scales. Our aims are to measure the spatial distribution and kinematics of the cold ISM/PDRs, and to compare this with the distribution and kinematics of star-forming regions traced by Hα (Jones et al. 2010). Although the delivered data did not meet our requested sensitivity, it is sufficient to examine the average ISM/PDR properties from the integrated [C II] emission.

Our source was observed by 25 antennas in band 9 during a ∼1 h track including calibration scans on the 31st of December 2012. Projected baseline lengths range from 13 to 376 m. The correlator was set up to obtain 4 spectral sub-bands of 2 GHz with 128 channels of 15.625 MHz. The receivers were tuned to center the bands on the following frequencies in GHz: 628.826, 630.520, 632.220 and 648.234. Passband, flux and phase calibrations used the quasar J0423-013, extrapolating from ALMA band 3 (∼100 GHz) and band 7 (∼300 GHz) observations made between December 14−16, 2012, which leads to a relatively large uncertainty, of the order of ∼25%, for the flux calibration. The visibilities were calibrated and the image cleaned with the CASA software. With natural weighting the clean beam full width at half maximum (FWHM) is $0.33'' \times 0.34''$ and the noise rms is $\sigma = 9.8$ mJy beam^{-1} in 14.9 km s^{-1} channels.

Flagging bad channels and masking out the [C II] 158 μm line, we integrate the four sub-bands to produce a continuum map, and obtain a noise of $\sigma_{\rm cont} = 0.84$ mJy beam^{-1}. No continuum emission is detected at the position of the gravitational arc. Integrating the flux in a box encompassing the arc as shown in the Fig. 1 and correcting for the primary beam, we obtain a 3σ upper limit of <27 mJy, which is compatible with the SPIRE 500 μm band (Zamojski et al., in prep.).

Integrating the spectra corrected for the primary beam in the same spatial box, we clearly detect the [C II] 158 μm line shown in Fig. 2. The flux integrated in the range 630.5−631.0 GHz is $S_{\rm CII} = 37.7 \pm 3.7$ Jy km s^{-1}, which corresponds to an intrinsic luminosity of $L_{\rm [CII]} = 1.2 \times 10^8\ L_\odot$, after correction for magnification by a factor $\mu = 49$. This magnification corresponds both to the mean magnification of the total arc (cf. Jones et al. 2010) and to the mean over the region concerned here, as determined from an updated version of the lensing model by Richard et al. (2011) and recent updates to it. We estimate an uncertainty of $\mu = 49 \pm 5$. Spatially, the [C II] emission closely follows the arc, as traced by the 1.4 and 3.6 μm emission. Given that the [C II] emission is very compact along the direction perpendicular to the arc, the flux is thus well constrained by the baselines in that direction. Furthermore, the length of the arc is smaller than the primary beam and the corresponding baselines are well sampled. Therefore, the flux lost due to missing short spacings should be small, and negligible compared to the flux uncertainties quoted above.

2.2. Other observations

The CO(3−2) line was detected with the PdBI by Dessauges-Zavadsky et al. (2015). The emission originates from the southern part of the arc, i.e. the same region as targeted with ALMA. The CO flux translates to a lensing-corrected CO(1−0) luminosity of $L_{\rm CO} = (5.1 \pm 1.5) \times 10^4\ L_\odot$, assuming a factor $r_{3,1} = 0.57$ between the CO(3−2) and CO(1−0) line luminosities, and $\mu = 49$ (Dessauges-Zavadsky et al. 2015). The IR spectral energy distribution of the MACS J0451+0006 arc, based on *Spitzer* and *Herschel* observations, has been studied in detail by Sklias et al. (2014), from which we obtain the IR luminosity for the southern part of the arc[1] corresponding to the region of the CO and [C II] detection. The CO and

[1] From the difference between the total luminosity and that of the subdominant northern part.

Table 1. Measured [C II] 158 μm and other key properties of the strongly lensed arc in MACS J0451+0006.

Quantity	Value
z^a	2.013
$\nu_{\rm CII}$	630.743 ± 0.015 GHz
$S_{\rm CII}{}^b$	37.7 ± 3.8 Jy km s^{-1}
$L_{\rm [CII]} \times \mu$	$(5.94 \pm 0.6) \times 10^9$ $L_\odot$
$L_{\rm [CII]}{}^b$	$(1.21 \pm 0.12) \times 10^8$ $L_\odot$
$L_{\rm IR}{}^c$	$(1.1-1.3) \times 10^{11}$ $L_\odot$
$L_{\rm FIR}{}^d$	$(0.5-0.9) \times 10^{11}$ $L_\odot$
$L_{\rm CO}{}^e$	$(5.1 \pm 1.5) \times 10^4$ $L_\odot$

Notes. The intrinsic luminosities are determined adopting the magnification factor $\mu = 49$ from the updated lens model of Richard et al. (2011). [(a)] Hα redshift from Richard et al. (2011). [(b)] Formal error, excluding ~25% systematic uncertainty from flux calibration. [(c)] IR luminosity of the S of the arc (cf. Sklias et al. 2014). [(d)] Range of $L_{\rm FIR}$ characterizing uncertainty in spatial separation of N and S arc. [(e)] From Dessauges-Zavadsky et al. (2015).

IR luminosities are listed in Table 1. As commonly used, $L_{\rm FIR}$ is defined as the luminosity between 42.5 and 122.5 μm rest frame, whereas the total IR luminosity, denoted $L_{\rm IR}$ here, refers to the 8−1000 μm domain.

Although both the CO and [C II] emission originate from the region, the two lines show different velocity profiles: the former, a double-peaked profile, and the latter, a single component centred on zero velocity. The apparent difference between the line profiles could result from the ISM properties of the galaxy or be due to the relatively low signal-to-noise of the CO line. Future ALMA observations should settle this question.

3. Results

3.1. Carbon emission from a z = 2, faint LIRG

We now compare the observed [C II] luminosity with that of other star-forming galaxies and AGN detected in the IR, both at low and high redshift. The [C II] 158 μm luminosity of MACS J0451+0006 is shown in Fig. 3, as a function of $L_{\rm FIR}$ together with previous detections in nearby and high-redshift galaxies and AGN. Two main results are clearly seen from this figure. First, our source has a significantly lower IR luminosity than previously studied galaxies at $z \gtrsim 1-2$. Indeed, thanks to a high magnification by gravitational lensing our source is currently the IR-faintest galaxy detected in [C II] 158 μm at $z > 1$, namely a faint LIRG. Second, relative to $L_{\rm FIR}$, the [C II] 158 μm emission of MACS J0451+0006 is $L_{\rm [CII]}/L_{\rm FIR} \approx (0.6.-1.2) \times 10^{-3}$, similar to that in nearby galaxies, as seen e.g. by the comparison with the measurements from Malhotra et al. (2001) and Sargsyan et al. (2012).

Although other [C II] measurements currently available for high-redshift ($z \gtrsim 2$) galaxies are mostly restricted to the very IR luminous objects ($L_{\rm IR} > 10^{12}$ $L_\odot$), the relative $L_{\rm [CII]}/L_{\rm FIR}$ emission of many of them is also comparable to that of MACS J0451+0006, as can be seen from Fig. 3. This is also the case for a Lyman break galaxy (LBG) at $z = 5.3$ from which Riechers et al. (2014) have recently detected [C II] emission with ALMA. Indeed, although the LBG is undetected in the IR continuum ($L_{\rm FIR} \lesssim 5.3 \times 10^{11}$ $L_\odot$[2]), [C II] is fairly strong, corresponding to $L_{\rm [CII]}/L_{\rm FIR} > 10^{-2.5}$. So far, the available data at $z \gtrsim 2$ show a fairly large dispersion in the $L_{\rm [CII]}/L_{\rm FIR}$ ratio, Some galaxies (marked with B14 in our figure) with high ratios of $L_{\rm [CII]}/L_{\rm FIR} \gtrsim 10^{-2}$ were recently found by Brisbin et al. (2015). However, most of their [C II] detections are of low significance, hence associated with large uncertainties.

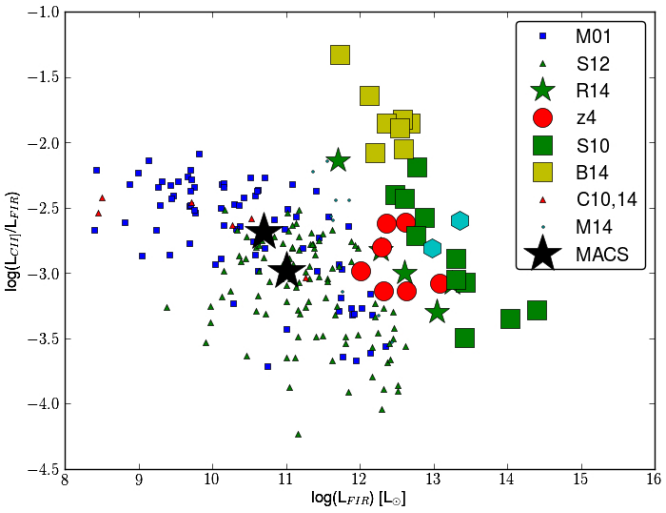

Fig. 3. Ratio of [C II] 158 μm over FIR luminosity, $L_{\rm [CII]}/L_{\rm FIR}$, versus $L_{\rm FIR}$ for MACS J0451+0006 (large, black stars) and comparison samples, which are detected both in [C II] and in the dust continuum. For MACS J0451+0006, the two points are meant to illustrate the uncertainties from $L_{\rm FIR}$, μ, and the band 9 calibration. Small symbols show nearby galaxies and AGN, large symbols sources at $z > 2$ from the following papers: M01: Malhotra et al. (2001), S12: Sargsyan et al. (2012), S10: Stacey et al. (2010), B14: Brisbin et al. (2015), C10,14: Cormier et al. (2010), Cormier et al. (2014), M14: Magdis et al. (2014), R14: Rawle et al. (2014), and z4: individual $z > 4$ galaxies (cf. Casey et al. 2014, and references therein).

The large scatter in [C II]/$L_{\rm FIR}$ probably implies that several factors, such as the average radiation field density, ISM density, metallicity, and others, determine the [C II]/FIR ratio, as amply discussed in the literature (e.g. Graciá-Carpio et al. 2011; Magdis et al. 2014). For the MACS J0451+0006 arc observed here, we have derived fairly detailed information on its stellar content, star formation rate, and dust properties, as well as some measure of its molecular gas (cf. Sklias et al. 2014; Dessauges-Zavadsky et al. 2015, and below). The dust temperature $T_{\rm d}$, in particular, has also been determined from our *Herschel* observations, and is found to be fairly high, between ~50−80 K, for the southern part of the arc observed here. Although local galaxies show an anti-correlation between the $L_{\rm [CII]}/L_{\rm FIR}$ ratio and $T_{\rm d}$ (cf. Malhotra et al. 2001; Graciá-Carpio et al. 2011; Magdis et al. 2014), our galaxy shows a "normal" ratio despite its high dust temperature. A similar result is also found for the $z = 2.957$ lensed galaxy HLSW-01 (SWIRE6) reported by Magdis et al. (2014), which has a high $T_{\rm d} = 51 \pm 2$ K and a normal ratio $L_{\rm [CII]}/L_{\rm FIR} = 1.5 \times 10^{-3}$. Clearly, more measurements and additional information on the physical properties of a representative sample of high-z galaxies are needed to improve our understanding of these objects and their ISM.

Given the agreement of the observed $L_{\rm [CII]}/L_{\rm FIR}$ with that of nearby objects, our galaxy is logically also in good agreement with the SFR–$L_{\rm [CII]}$ relation (cf. de Looze et al. 2011; De Looze et al. 2014) determined from local star-forming galaxies. Indeed, from $L_{\rm IR}$ the star formation rate is SFR(IR)= 11−13 $M_\odot$ yr^{-1} for a Chabrier/Kroupa IMF, one would obtain $L_{\rm [CII]} = (1.5-1.8) \times 10^8$ $L_\odot$, in fair agreement with our observed value.

[2] 3σ limit obtained from their Table 1.

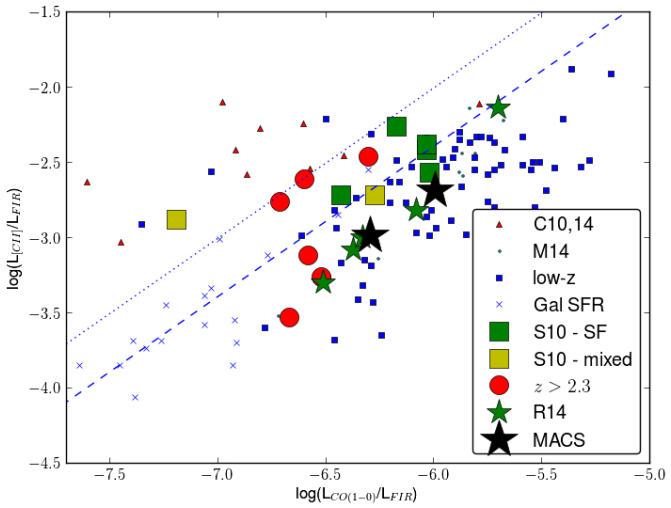

Fig. 4. $L_{[CII]}/L_{FIR}$ versus L_{CO}/L_{FIR} with MACS J0451+0006 (large, black stars; cf. Fig. 3) and other samples. Small symbols show low-z star-forming galaxies and AGN, large symbols $z > 2$ galaxies from the following papers: C10,14: Cormier et al. (2010); Cormier et al. (2014), M14: Magdis et al. (2014), S10: Stacey et al. (2010), R14: Rawle et al. (2014), and various $z > 2$ galaxies from the literature. Crosses show Galactic SF regions with low IR luminosities below the range plotted in Fig. 3. The dashed (dotted) line shows a ratio of $L_{[CII]}/L_{CO} = 4.1 \times 10^3$ (10^4).

3.2. Normal [C II]/CO emission

The [C II] 158 μm and CO line strengths, both normalized to L_{FIR}, are shown in Fig. 4 and compared to available data from nearby and distant galaxies and AGN. Again MACS J0451+0006 is found in a region of "normal" [C II]/CO ratios, close to $L_{[CII]}/L_{CO} = 4.1 \times 10^3$ shown by the dashed line, where most nearby starbursts, AGN, and $z \sim 1-2$ star-forming galaxies are found. In contrast, nearby quiescent star-forming galaxies show a lower [C II]/CO ratio (Stacey et al. 2010). At the other end, some objects, mostly dwarf galaxies, show significantly higher [C II]/CO ratios, exceeding significantly $L_{[CII]}/L_{CO} = 10^4$.

Both observations and PDR modeling suggest that high [C II]/CO ratios are related to low metallicity (cf. Stacey et al. 1991, Cormier et al. 2010, De Breuck et al. 2011). High [C II]/CO ratios are explained by spherical PDR models, where the CO emission region is reduced at low metallicity (see e.g. Bolatto et al. 1999; Röllig et al. 2006). For MACS J0451+0006, Richard et al. (2011) derive a metallicity of 12 + log(O/H) = $8.80^{+0.13}_{-0.12}$ from the [N II]/Hα ratio. However, since the region may contain an AGN (Zamosjki et al., in prep.), [N II]/Hα may be boosted by the AGN and the metallicity hence overestimated. Indeed, a low/sub-solar metallicity would be expected from the fairly low mass of this galaxy. Using e.g. the fundamental mass-SFR-metallicity relation of Mannucci et al. (2010), one expects 12 + log(O/H) $\approx$ 8.4, which is lower than the above estimate. However, in comparison to the nearby dwarf galaxies from Cormier et al. (2010, 2014), with metallicities 12 + log(O/H) = 7.89−8.38, MACS J0451+0006 has a higher metallicity, consistent with a lower [C II]/CO ratio.

Compared to most low-redshift galaxies (except for low-metallicity dwarf galaxies), MACS J0451+0006 shows a comparable L_{CO}/L_{FIR} ratio (Fig. 4), although a large dispersion is found at all redshifts (cf. Genzel et al. 2010; Combes et al. 2013; Dessauges-Zavadsky et al. 2015). At the corresponding L_{IR}/L_{CO} (or equivalently L_{IR}/M_{H_2}) ratio, the observed $L_{[CII]}/L_{FIR}$ ratio is slightly below than, although consistent with, the observed trend of local galaxies (Graciá-Carpio et al. 2011; Magdis et al. 2014).

In simple 1D PDR models, the main physical parameters are the incident far-UV (FUV) radiation field, commonly measured by the Habing flux G_0, and the gas density (e.g. Le Petit et al. 2002). From such models, variations of L_{CO}/L_{FIR} are mostly explained by varying G_0, with an increased FUV flux causing a decrease of L_{CO}/L_{FIR} (cf. Stacey et al. 1991, 2010). In their $z \sim 1-2$ galaxy sample, Stacey et al. (2010) find that galaxies containing an AGN have on average a higher FUV flux, i.e. a lower L_{CO}/L_{FIR} ratio. Indeed, MACS J0451+0006 shows a L_{CO}/L_{FIR} ratio comparable to their $z \sim 1-2$ "mixed" sample, which could indicate that the ratio is also affected by a presumed AGN contribution in this galaxy. However, the comparison sample of Stacey et al. (2010) is very small, and other galaxies at high redshift (indicated as $z > 2.3$ in Fig. 4) also display comparable properties in the $L_{[CII]}/L_{FIR}$ and L_{CO}/L_{FIR} ratios.

3.3. Discussion

To place our target into a more general context of IR-detected galaxies, MACS J0451+0006 is, with $L_{IR} = (1.1-1.3) \times 10^{11}\ L_\odot$, a faint LIRG. This infrared luminosity, $L_{IR} \sim 0.3-0.4 L^\star$, is below the characteristic value of $L^\star$ at $z = 2$, using the luminosity function of Gruppioni et al. (2013), or at $\sim 0.07 L^{knee}$ using the measurements of Magnelli et al. (2013). Compared to the stellar mass function of star-forming galaxies at $z \sim 2$, our galaxy has a mass of $\sim 0.031\ M^\star$ (cf. Ilbert et al. 2013).

Compared to other galaxies currently detected in [C II] at high redshift, for which information is relatively sparse, our rich data set available for MACS J0451+0006 allow us to determine quantities concerning its dust content (mass, temperature, UV attenuation), gas content (CO mass, gas depletion timescale, gas fraction), stellar content (SFR, mass, approximate metallicity), and kinematics (see Jones et al. 2010; Richard et al. 2011; Sklias et al. 2014; Dessauges-Zavadsky et al. 2015). From our present knowledge at $z \sim 2$, MACS J0451+0006 appears as fairly normal for its stellar and star formation properties: it is e.g. close to or within the main sequence of Daddi et al. (2007), although this not well determined in the mass range of MACS J0451+0006. In terms of ISM/PDR properties, however, only a few galaxies are measured at these redshifts, preventing us from determining what their "normal"/typical properties are. In any case, despite a higher sSFR and hotter dust compared to nearby galaxies and possibly the presence of an AGN, MACS J0451+0006 shows relative [C II] 158 μm/IR and CO/IR properties, which are very similar to those of nearby (and few other $z \sim 1-2$) star-forming galaxies. This shows that the ISM properties depend in a more complex manner on several physical parameters.

4. Conclusion

Using ALMA in cycle 0, we detected [C II] 158 μm emission from the $z = 2.013$ strongly lensed, multiply-imaged arc MACS J0451+0006 previously studied in depth thanks to HST, *Spitzer*, *Herschel*, and IRAM observations. The spatially integrated [C II] luminosity corresponds to $L_{[CII]} = 1.2 \times 10^8\ L_\odot$, after correction for lensing. The IR luminosity of this galaxy is ~10 times fainter than any previous source detected both in [C II] and in the IR continuum at high redshift. The observed ratio of [C II]-to-IR emission, $L_{[CII]}/L_{FIR} \approx (1.2-2.4) \times 10^{-3}$, is found to be similar to that in nearby galaxies. The same also holds for the observed [C II]/CO ratio, which is comparable to

that of star-forming galaxies and AGN at low redshift, and also in agreement with available measurements in more IR-luminous systems at high redshift. Although MACS J0451+0006 shows a high dust temperature ($T_d \gtrsim 50$ K, Sklias et al. 2014), the $L_{[CII]}/L_{FIR}$ ratio is not lower than in nearby galaxies with comparable dust temperatures (cf. Malhotra et al. 2001; Magdis et al. 2014).

Our previous CO observations with IRAM and the present [C II] 158 μm detection with ALMA provide a first hint on PDR/ISM properties of a relatively low-mass ($M_\star \sim 2.5 \times 10^9\ M_\odot$) star-forming galaxy at $z \sim 2$. Observations of larger samples of "normal" star-forming galaxies at high redshift should soon become available, providing us with a better understanding of their ISM and star formation properties. Further ALMA observations of MACS J0451+0006 have been approved to study [C II], CO, and dust emission on small spatial scales down to ~200 pc in the source plane.

Acknowledgements. This work was supported by the Swiss National Science Foundation. This paper makes use of the following ALMA data: ADS/JAO.ALMA#2011.0.00130.S. ALMA is a partnership of ESO (representing its member states), NSF (USA), and NINS (Japan), together with NRC (Canada) and NSC and ASIAA (Taiwan), in cooperation with the Republic of Chile. The Joint ALMA Observatory is operated by ESO, AUI/NRAO, and NAOJ. We gratefully thank the ALMA staff of NAASC for their assistance in preparing the observations, which form the basis of this Letter.

References

Bolatto, A. D., Jackson, J. M., & Ingalls, J. G. 1999, ApJ, 513, 275
Brisbin, D., Ferkinhoff, C., Nikola, T., et al. 2015, ApJ, 799, 13
Carilli, C. L., & Walter, F. 2013, ARA&A, 51, 105
Casey, C. M., Narayanan, D., & Cooray, A. 2014, Phys. Rep., 541, 45
Combes, F., García-Burillo, S., Braine, J., et al. 2013, A&A, 550, A41
Cormier, D., Madden, S. C., Hony, S., et al. 2010, A&A, 518, L57
Cormier, D., Madden, S. C., Lebouteiller, V., et al. 2014, A&A, 564, A121
Daddi, E., Dickinson, M., Morrison, G., et al. 2007, ApJ, 670, 156
De Breuck, C., Maiolino, R., Caselli, P., et al. 2011, A&A, 530, L8
De Breuck, C., Williams, R. J., Swinbank, M., et al. 2014, A&A, 565, A59
de Looze, I., Baes, M., Bendo, G. J., Cortese, L., & Fritz, J. 2011, MNRAS, 416, 2712
De Looze, I., Cormier, D., Lebouteiller, V., et al. 2014, A&A, 568, A62
Dessauges-Zavadsky, M., Zamojski, M., Schaerer, D., et al. 2015, A&A, in press DOI: 10.1051/0004-6361/201424661
Egami, E., Rex, M., Rawle, T. D., et al. 2010, A&A, 518, L12
Genzel, R., Tacconi, L. J., Gracia-Carpio, J., et al. 2010, MNRAS, 407, 2091
Graciá-Carpio, J., Sturm, E., Hailey-Dunsheath, S., et al. 2011, ApJ, 728, L7
Gruppioni, C., Pozzi, F., Rodighiero, G., et al. 2013, MNRAS, 432, 23
Ilbert, O., McCracken, H. J., Le Fèvre, O., et al. 2013, A&A, 556, A55
Jones, T. A., Swinbank, A. M., Ellis, R. S., Richard, J., & Stark, D. P. 2010, MNRAS, 404, 1247
Le Petit, F., Roueff, E., & Le Bourlot, J. 2002, A&A, 390, 369
Magdis, G. E., Rigopoulou, D., Hopwood, R., et al. 2014, ApJ, 796, 63
Magnelli, B., Popesso, P., Berta, S., et al. 2013, A&A, 553, A132
Malhotra, S., Kaufman, M. J., Hollenbach, D., et al. 2001, ApJ, 561, 766
Mannucci, F., Cresci, G., Maiolino, R., Marconi, A., & Gnerucci, A. 2010, MNRAS, 408, 2115
Rawle, T. D., Egami, E., Bussmann, R. S., et al. 2014, ApJ, 783, 59
Richard, J., Jones, T., Ellis, R., et al. 2011, MNRAS, 413, 643
Riechers, D. A., Bradford, C. M., Clements, D. L., et al. 2013, Nature, 496, 329
Riechers, D. A., Carilli, C. L., Capak, P. L., et al. 2014, ApJ, 796, 84
Röllig, M., Ossenkopf, V., Jeyakumar, S., Stutzki, J., & Sternberg, A. 2006, A&A, 451, 917
Saintonge, A., Lutz, D., Genzel, R., et al. 2013, ApJ, 778, 2
Sargsyan, L., Lebouteiller, V., Weedman, D., et al. 2012, ApJ, 755, 171
Sklias, P., Zamojski, M., Schaerer, D., et al. 2014, A&A, 561, A149
Stacey, G. J., Geis, N., Genzel, R., et al. 1991, ApJ, 373, 423
Stacey, G. J., Hailey-Dunsheath, S., Ferkinhoff, C., et al. 2010, ApJ, 724, 957
Tacconi, L. J., Genzel, R., Neri, R., et al. 2010, Nature, 463, 781